Advances in Clinical Radiology 1 (2019) 55–69
ADVANCES IN CLINICAL RADIOLOGY

Quantitative MRI Biomarkers of Diffuse Liver Disease

Michael C. Olson, MD[a], Scott B. Reeder, MD, PhD[a,b,c,d,e], Sudhakar K. Venkatesh, MD[f,*]

[a]Department of Radiology, Wisconsin Institutes for Medical Research, University of Wisconsin–Madison, 1111 Highland Avenue, Madison, WI 53705, USA; [b]Department of Medical Physics, University of Wisconsin–Madison, Madison, WI, USA; [c]Department of Biomedical Engineering, University of Wisconsin–Madison, Madison, WI, USA; [d]Department of Medicine, University of Wisconsin–Madison, Madison, WI, USA; [e]Department of Emergency Medicine, University of Wisconsin–Madison, Madison, WI, USA; [f]Department of Radiology, Mayo Clinic College of Medicine, Mayo Clinic, 200 First Street Southwest, Rochester, MN 55905, USA

KEYWORDS

• Noninvasive quantitative biomarkers • Chemical shift–encoded MRI (CSE-MRI)
• Magnetic resonance elastography (MRE) • Proton density fat fraction (PDFF) • R2* • Steatosis • Fibrosis

KEY POINTS

- There has been growing interest in the development of noninvasive biomarkers for the diagnosis, quantification, and monitoring of patients with hepatic steatosis and fibrosis.
- Chemical shift–encoded MRI is a confounder-corrected technique that allows quantification of hepatic fat and iron content in the form of proton density fat fraction and R2*, respectively.
- Magnetic resonance elastography can be used to accurately diagnose and stage hepatic fibrosis.

INTRODUCTION

Affecting an estimated 60 million to 100 million adults, nonalcoholic fatty liver disease (NAFLD) is the most common cause of chronic liver disease in the US [1]. NAFLD is an umbrella term encompassing a spectrum of disorders ranging from isolated steatosis (nonalcoholic fatty liver) to steatohepatitis (nonalcoholic steatohepatitis [NASH]) [2–4]. NAFLD is associated with obesity, diabetes, and the metabolic syndrome and is predicted to be a major health care burden and the most common indication for liver transplantation in the future [5]. In its advanced stages, NAFLD can progress to end-stage liver disease and cirrhosis. Estimated to affect up to 1% of the population worldwide and more than 600,000 adults in the United States alone [6,7], cirrhosis develops in response to chronic hepatic injury and is characterized histologically by the formation of regenerative nodules and fibrosis [6]. A substantial cause of morbidity and mortality, cirrhosis predisposes patients to the development of complications, such as portal hypertension, ascites, varices, hepatic encephalopathy, bacterial infections, disordered clotting, and hepatocellular carcinoma [8]. Previously believed irreversible, hepatic fibrosis may

Disclosure Statement: M.C. Olson and S.K. Venkatesh: No disclosures. S.B. Reeder: No relevant disclosures. Unrelated: Ownership in Calimetrix, Reveal Pharmaceuticals, Elucent Medical, and Cellectar Biosciences. The authors wish to acknowledge support from the NIH (R01 DK083380, R01 DK088925, R01 DK100651, and K24 DK102595) as well as GE Healthcare, who provide research support to the University of Wisconsin–Madison. Furthermore, S.B. Reeder is a Romnes Faculty Fellow and has received an award provided by the University of Wisconsin–Madison Office of the Vice Chancellor for Research and Graduate Education with funding from the Wisconsin Alumni Research Foundation.

*Corresponding author, *E-mail address:* Venkatesh.sudhakar@mayo.edu

https://doi.org/10.1016/j.yacr.2019.04.009
2589-8744/19/

regress with therapy and intervention in early stages [9,10]. As a result, prompt recognition of both hepatic steatosis and fibrosis is of paramount importance in the prevention and treatment of chronic liver disease and cirrhosis.

Historically, the accepted reference standard for the diagnosis and staging of hepatic steatosis and fibrosis was histologic assessment of tissue obtained from liver biopsy. Liver biopsy is invasive, however, and can be complicated by pain and bleeding, reported in up to 84% and 0.2% of procedures, respectively [11]. Fatal hemorrhage has been described in a small but nontrivial number of cases, with a risk of 1/10,000 [11]. In addition, liver biopsy is prone to sampling error, because a typical tissue specimen may represent only 1/50,000 of total liver mass [12–14]. These drawbacks highlight the unmet need for noninvasive means of diagnosing, grading, and staging disease features, such as steatosis and hepatic fibrosis. Panels of serum markers and noninvasive algorithms can reliably exclude cirrhosis and prevent unnecessary biopsies but currently are unreliable for the diagnosis and staging of early fibrosis [15,16].

Within the past decade, chemical shift–encoded (CSE) MRI and magnetic resonance elastography (MRE) have emerged as advanced imaging techniques capable of accurately and reproducibly diagnosing and quantifying hepatic steatosis and fibrosis [1,17–22]. As these technologies are increasingly incorporated into routine clinical practice, it will be important for practicing radiologists to understand the utility of these techniques, the interpretation and analysis of the images they generate, and the limitations of and common pitfalls encountered with their use. The goal of this review is to provide practicing radiologists with an overview of emerging quantitative MRI biomarkers of diffuse liver disease.

EVALUATION OF HEPATIC FAT CONTENT

Defined as the abnormal intracellular accumulation of triglycerides within hepatocytes, hepatic steatosis is the defining and hallmark feature of NAFLD. The presence of steatosis can incite an inflammatory response that, through mechanisms that remain unclear, results in progression to NASH and its manifold complications, including the development of cirrhosis, liver failure, and hepatocellular carcinoma. Moreover, recent evidence indicates that the pathologic manifestations of hepatic steatosis extend well beyond the liver. One recent analysis found that steatosis, as documented on noncontrast CT, had a stronger association with significant coronary artery disease than more traditionally well-recognized risk factors, such as hypertension, diabetes, and smoking [23]. Among patients with NAFLD, cardiovascular disease actually accounts for a higher proportion of mortality (25%) than does liver disease (13%) [5]. Furthermore, steatosis occurs prior to insulin resistance, providing indirect evidence that steatosis may play a causative role in the development of both type 2 diabetes mellitus and the metabolic syndrome rather than develop as the hepatic manifestation of these conditions [24–26].

Conventionally, diagnosis of hepatic steatosis has been established through histopathologic analysis, with disease severity scored on a scale of 0 to 3 based on the number hepatocytes containing intracellular fat vacuoles (grade 0, less than 5%; grade 1%, 5%–33%; grade 2%, 34%–66%; and grade 3, >67%) [27]. This histopathologic evaluation is an inherently 2-D measurement of a small section of 3-D hepatic parenchyma and may not be truly representative of overall liver fat content. Recent evidence has shown that this method of diagnosis and staging is subject to wide interobserver variability and poor reproducibility [28].

Given the inherent risks of serial liver biopsy and the important limitations of histopathologic analysis, there has been growing interest in the development of noninvasive quantitative biomarkers for the diagnosis, quantitative grading, and longitudinal monitoring of patients with hepatic steatosis.

MRI EVALUATION OF HEPATIC FAT CONTENT

Magnetic resonance spectroscopy (MRS) and conventional MRI have been used to detect the presence of hepatic fat for decades (Table 1). MRS relies on knowledge of the resonant frequencies of fat and water protons, which are depicted on a spectral tracing. The signal intensities of the protons at these respective frequencies are quantified, allowing for determination of the signal fat fraction [22]. Although extremely sensitive to hepatic fat content and widely accepted as an accurate means of noninvasive fat quantification [29–32], MRS is a highly specialized, time-intensive technique that is limited by small sample volumes (problematic in heterogeneous livers and for longitudinal assessment) and an inability to be performed online at the time of image acquisition [1,22,33].

Conventional imaging sequences, such as fat-suppression techniques and in-phase and opposed-phase imaging [34], also take advantage of the different resonance frequencies of fat and water to resolve the

TABLE 1
Limitations of Conventional MRI Evaluation of Hepatic Fat Content

Method	Limitations
MRS	• Highly specialized and time intensive • Small sample volumes • Cannot be performed online at time of image acquisition
Fat-suppression sequences	• Incomplete or inhomogeneous suppression of fat signal • Unintentional suppression of water signal
In-phase and opposed-phase sequences	• Measurement of signal fat fraction confounded by several factors ○ T1 bias ○ T2* decay ○ Spectral complexity of fat ○ Noise bias ○ Eddy currents

signal generated by the liver into its fat and water components. With fat suppression, 2 sets of images are acquired. In 1, fat signal is suppressed with the use of fat-saturation pulses; image acquisition parameters otherwise are identical. The signal intensities of the 2 sets of images are compared, with the difference in intensity assumed attributable to fat.

Measurement of signal fat fraction is confounded, however, by several factors, including T1 bias, T2* decay, spectral complexity of fat, noise bias, and eddy currents, and may be poorly reflective of the true hepatic fat content. A comprehensive overview of these techniques and confounders is beyond the scope of this review but can be found elsewhere in the literature [21,22].

QUANTITATIVE CHEMICAL SHIFT–ENCODED MRI

As discussed previously, magnetic resonance techniques that measure signal fat fraction are subject to an array of biological and technological confounding factors, precluding accurate, repeatable, and reproducible measurement of hepatic fat content. If these confounding factors are avoided or accounted for, the signal fat fraction becomes equivalent to the proton density fat fraction (PDFF), defined as the density of mobile protons in triglycerides relative to the total mobile proton density [22,33].

CSE-MRI is a confounder-corrected technique that utilizes image acquisition at 2 or more echo times to divide the magnetic resonance signal into fat and water components. The 2 confounder-corrected advanced MRI techniques used to quantify PDFF can be characterized as either magnitude-based or complex-based. The magnitude-based technique foregoes phase information and consists of magnitude images obtained at multiple echo times (3 or more, typically 6) where water and fat signal are in phase and out of phase [35–43], allowing for estimation of fat fraction ranging from 0% to 50%. This limitation may prevent evaluation of fat fraction in predominantly fatty tissues, such as adipose or marrow, although the clinical relevance is doubtful—hepatic PDFF values exceeding 50% do occur but are rare.

The complex-based method [44–49] relies on both phase and magnitude data and allows for comprehensive evaluation of fat fraction with a dynamic range of 0% to 100%. Phase and magnitude information is derived from 3 or more images (typically 6) acquired at optimized echo times that allow the separation of fat and water signals.

An added benefit of CSE-MRI techniques is that the same data set used to produce a PDFF-based estimate of hepatic fat content can simultaneously generate an estimate of confounder-corrected liver iron content in the

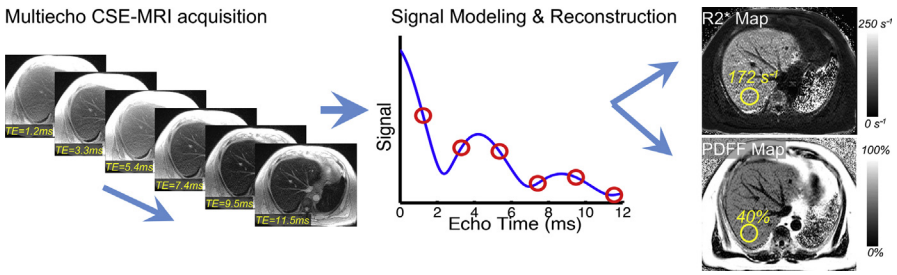

FIG. 1 Generation of parametric maps. Data points are acquired from a multiecho CSE-MRI acquisition and fitted to a signal model, allowing estimation of R2* and PDFF on a pixel-by-pixel basis. TE, echo time.

form of R2* (1/T2*) [50,51] (Fig. 1). R2* is the rate of signal decay in the liver. Conditions that result in excess iron accumulation, such as hereditary hemochromatosis and hematologic disorders necessitating serial blood transfusions, can cause liver injury that progresses to fibrosis and cirrhosis. Furthermore, numerous chronic liver disease, including NAFLD, can precipitate iron overload, the development of which can contribute to disease progression [52].

PROTON DENSITY FAT FRACTION AND R2* MAPS

Most commonly, CSE-MRI data are obtained using a 20-second breath-hold with a 3-D acquisition of the whole liver. From this acquisition, a parametric map can automatically be reconstructed by the scanner computer, typically in a few seconds. This provides a visual representation of hepatic PDFF, expressed as a percentage; this fundamental tissue property serves as a surrogate for the underlying triglyceride concentration throughout the liver.

Correspondingly, the same acquisition can be used to generate an R2* map, which provides a fat-corrected estimate of hepatic iron content in the form of R2* [53] (Fig. 2). R2* is directly proportional to liver iron content (milligrams of iron/grams of dry liver) and is measured in units of 1/s [52]. Regions of interest (ROIs) can be placed throughout the hepatic parenchyma on the PDFF and R2* maps to produce quantitative estimates of liver fat and iron content, respectively.

Within the literature, significant variability exists with respect to the technique by which to measure PDFF and R2* from ROIs. Differences arise in the size of the ROIs used (ranging from approximately 1 cm to 3 cm), the number of ROIs drawn (2 to 9), and the location in which the ROIs are placed (lobe vs individual Couinaud segments), among other factors [54–60]. Nonuniformity in measurement techniques may affect comparison of quantitative values across centers adversely. A recent analysis by Campo and colleagues [61] examined the reproducibility and repeatability of PDFF and R2* measurements using ROIs of different sizes (1 cm^2, 4 cm^2, and largest possible) placed in different locations throughout the liver (from 1 in each lobe to 1 in each of the 9 Couinaud segments), concluding that inter-reviewer and intra-reviewer agreement was maximized by sampling the greatest possible liver volume via a large number of large ROIs, albeit at the expense of increased analysis time. Thus, the most efficient approach may be to place either 1 large (4 cm^2 or greater) ROI in either each of the 9 Couinaud segments or in the medial, lateral, anterior, and posterior hepatic segments [61].

Potential pitfalls with ROI placement include water-fat swapping, particularly near the hepatic dome, which is caused by magnetic field inhomogeneities. Such

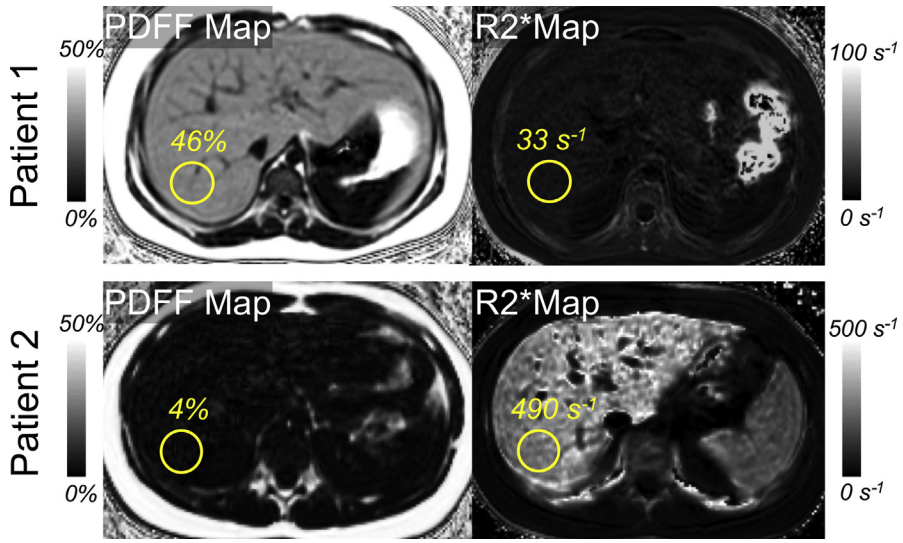

FIG. 2 Top row: Patient 1. PDFF map (*left*) shows severe steatosis and R2* map (*right*) shows normal liver iron content. Bottom row: Patient 2. PDFF map (*left*) shows normal fat content R2* map (*right*) shows iron overload. Yellow circles are region of interest drawn and numbers are the measurements obtained. PDFF is expressed as percentage and R2* is expressed as s-1.

swaps corrupt both PDFF and R2* measurements. Motion or ghosting may render measurements invalid, and areas of obvious artifact also should be avoided; similarly, blood vessels can create flow-related artifacts that are not readily apparent, and placement of ROIs within the hepatic vasculature is not recommended. In cases of severe iron overload, the PDFF value may not be valid [53]; the calculated R2* is valid but less precise and less accurate, making comparison across serial examinations difficult.

APPLICATIONS

As discussed previously, the histopathologic diagnosis of hepatic steatosis can be made when the number of hepatocytes containing intracellular fat vacuoles exceeds 5% (Box 1) [27]. The widely cited PDFF threshold separating normal from abnormal of 5.56% is based on a seminal investigation by Szczepaniak and colleagues [62], who defined this cutoff as the 95th percentile as measured in 345 patients with no risk factors for steatosis as part of the Dallas Heart Study. This cutoff value, however, has little basis in determining the presence or absence of disease. Recent evidence suggests that a PDFF threshold of as low as 2% to 3% may be predictive of hepatic steatosis and the metabolic syndrome [56,63]. As such, noninvasive quantitative biomarkers must be able to provide precise, accurate, repeatable, and reproducible estimates of hepatic fat content, especially at low concentrations, to allow for accurate diagnosis and assessment of small changes in fat content in response to treatment.

Like histopathologic analysis, MRS can be subject to sampling error; the signal typically is acquired within a small voxel measuring approximately 2 cm^3 × 2 cm^3 × 2 cm^3, and steatosis can be heterogeneously distributed throughout the liver [64]. MRS, too, requires time-intensive postprocessing and a high degree of expertise.

BOX 1
Applications of Chemical Shift–Encoded MRI

- Diagnosis and quantification of hepatic steatosis and iron overload
- Longitudinal monitoring of hepatic fat and iron content
  - Serial follow-up over time
  - Response to medical or surgical therapy
- Rapid, cost-effective imaging protocols can be used to quickly determine hepatic fat and iron content

A recent meta-analysis encompassing 28 studies and approximately 2000 subjects demonstrated excellent correlation between PDFF measurements of hepatic fat fraction and MRS [33]. Validated in both phantoms and animals [40,65,66], confounder-corrected CSE-MRI techniques can be used to calculate precise, accurate, and reproducible estimates of PDFF regardless of field strength, vendor, or platform, and can be used in both children and adults [41,56,67,68]. Imaging of the entire liver eliminates challenges associated with heterogeneity of fat deposition [64], and with a dynamic range of 0% to 100%, CSE-MRI can be used to accurately quantify clinically relevant steatosis [1] (Fig. 3).

Given its excellent repeatability and reproducibility, PDFF measured by CSE-MRI can be used to monitor changes in hepatic fat content across serial examinations in patients who achieve substantial weight loss or those who undergo pharmacologic or surgical therapy [1,22] (Fig. 4).

Based on the rapidity with which CSE-MRI sequences can be acquired, it may be possible to devise limited imaging protocols that allow for determination of hepatic fat content at a cost similar to that of a panel of laboratory tests [64] (Box 2). Recent guidelines have indicated the appropriate billing of fat quantification methods as a limited MRI examination. Based on a recent search on CMS.gov, the global fee for a limited examination is approximately $290.

Because PDFF and R2* maps can be generated concurrently from a CSE-MRI acquisition, many of the concepts, enumerated previously, also apply to hepatic iron quantification. The use of confounder-corrected R2* allows accurate noninvasive diagnosis, staging, and longitudinal monitoring of hepatic iron overload [52].

LIMITATIONS

At present, CSE-MRI techniques are based on multiecho, spoiled gradient-echo sequences, which can be adversely impacted by motion artifact; the ghosting of subcutaneous fat into the liver, for example, can corrupt PDFF measurements of hepatic fat content (Box 3). Relatively long breath-holds are needed to minimize artifact, which may be problematic in children and patients with poor pulmonary function. Respiratory-gated and navigator-based sequences have been developed that allow for free breathing at the expense of greater table time with some residual artifact [58]. One recent study suggests that motion artifact may be all but eliminated with the use of a sequentially acquired 2-D CSE-MRI technique [69].

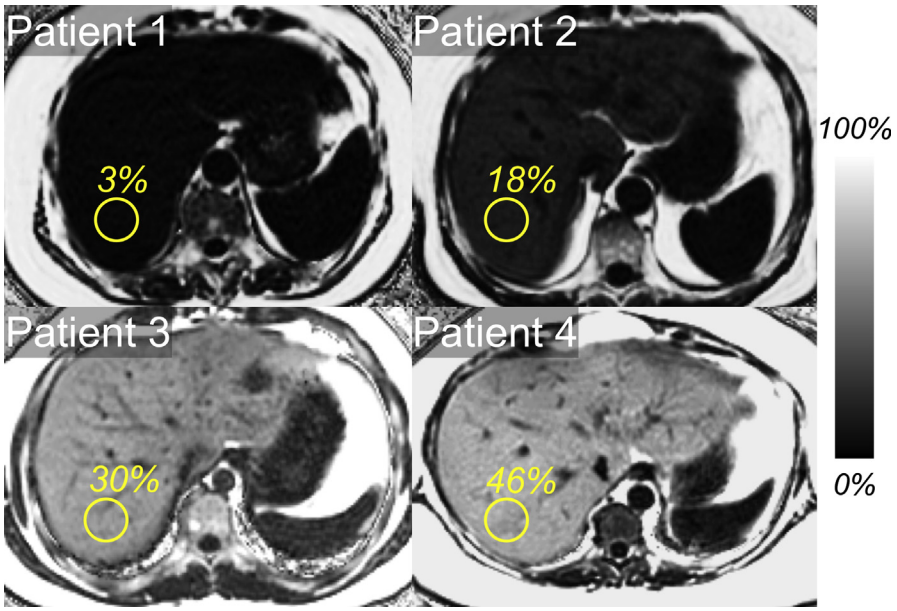

FIG. 3 PDFF maps in four different patients illustrating a wide range of hepatic fat content that can be depicted by PDFF maps (in this case, fat content ranging from 3% 46%). Yellow circles are region of interest drawn and numbers are the measurements obtained.

A recent large meta-analysis [33] demonstrated that CSE-MRI is accurate over a wide range of PDFF values but that its variability falls in the range of 3% to 4%. Some of this variability may be attributable to the low signal-to-noise ratio of current techniques. With recent evidence suggesting that PDFF values of as low as 3% may indicate clinically relevant steatosis [56], this degree of variability has a negative impact on the ability of current CSE-MRI techniques to recognize disease in patients with low hepatic fat content. Repeatability of CSE-MRI can be improved by increasing signal-to-noise ratio at the cost of minor reductions in spatial resolution without sacrificing measurement accuracy [70]. Future advancements will focus on the refinement of novel CSE-MRI approaches that enable accurate, precise quantification of fat in patients with early-stage disease.

EVALUATION OF HEPATIC FIBROSIS

Hepatic fibrosis is the endpoint of all chronic liver diseases, leading to destruction of parenchyma and inflammation. Hepatic fibrosis also is the single most important factor that determines outcome in chronic

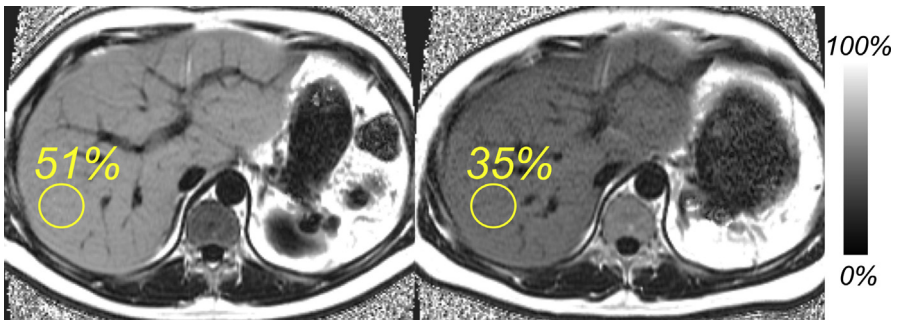

FIG. 4 Longitudinal monitoring of hepatic steatosis using PDFF maps. The left panel is the baseline PDFF map and the right panel is PDFF obtained after 3 months showing significant reduction in hepatic content after initiation of pharmacologic therapy.

BOX 2
Advantages of Chemical Shift–Encoded MRI

- Noninvasive
- Simultaneous calculation of PDFF and R2*
- Well validated, accurate, reproducible, and repeatable measurements of hepatic fat and iron content across field strengths and vendors
- Can be performed online at the time of image acquisition
- Allows imaging of the entire liver
  - Not subject to sampling error

liver diseases, including NAFLD [71]. Detection and staging of hepatic fibrosis, therefore, are of paramount importance. The reference standard for detection and staging of hepatic fibrosis is liver biopsy. Liver biopsy, however, is invasive and is associated with complications and limitations, as highlighted in the section on hepatic fat quantification, discussed previously. Noninvasive diagnosis and staging of hepatic fibrosis, therefore, is the preferred method. Currently, elastography methods are the imaging tests of choice for evaluation of hepatic fibrosis.

Elastography can be performed with either ultrasound or MRI, with MRE the most accurate noninvasive imaging-based method for detection and staging of hepatic fibrosis. Mean liver stiffness values as determined by MRE increase in stepwise fashion with increasing hepatic fibrosis [72,73]. There is a small incremental increase in MRE-measured liver stiffness in early stages of fibrosis and an exponential increase in stiffness with advanced fibrosis and beyond. This reflects the amount of collagen deposition (ie, fibrosis) in the liver at the histologic level. The stiffness of a normal liver is comparable to that of subcutaneous fat, generally measuring less than 2.5 kPa [74–76], whereas studies have shown that cirrhotic livers range in stiffness from 4.21 kPa to 8.02 kPa [73,77–80] (Table 2).

BOX 3
Limitations of Chemical Shift–Encoded MRI

- Based on multiecho spoiled gradient-echo sequences
  - Susceptible to motion artifact
- Requires relatively long breath holds
  - Potentially problematic in children and ill patients
- PDFF variability may be in the range of 3% to 4%
  - May have adverse impact on diagnosis of steatosis in patients with early disease

MAGNETIC RESONANCE EVALUATION OF FIBROSIS: MAGNETIC RESONANCE ELASTOGRAPHY

MRE can be performed on any standard clinical magnetic resonance scanner with the addition of specialized hardware and processing software. MRE consists of 3 fundamental steps: the introduction of mechanical shear waves into body tissue; the imaging of those waves with a dedicated MRI sequence; and the processing of phase shift information to derive shear-wave displacement images (wave images) to generate tissue stiffness maps (elastograms) [19,81,82].

MRE uses mechanical shear waves to quantitatively measure the stiffness of tissue [83], and this can be achieved on most clinical systems with an acoustic driver (active driver), situated outside the magnet room, to generate low-frequency waves (standard 60 Hz for hepatic applications). The acoustic waves are transmitted via plastic tubing to a passive pneumatic driver, which is secured with a nonmetallic strap to a patient's right anterior chest wall and upper abdomen, over the liver [19,82]. The passive driver generates shear waves in tissues whose amplitudes are highest near the body surface. Because shear waves propagate through the liver, imaging of the shear waves can be performed using any of a variety of motion-sensitive pulse sequences, including steady-state free precession, echo-planar imaging (EPI), gradient-recalled-echo (GRE),

TABLE 2
Magnetic Resonance Elastography Thresholds for Hepatic Fibrosis

Stage of Fibrosis	Hepatic Stiffness (kPa)
Normal	<2.5
Normal or inflammation	2.5–3.0
Stage 1–2	3.0–3.5
Stage 2–3	3.5–4.0
Stage 3–4	4.0–5.0
Stage 4 or cirrhosis	>5.0

Adapted from Venkatesh SK, Ehman RL. Magnetic resonance elastography of liver. Magn Reson Imaging Clin N Am 2014;22(3):440; with permission.

and spin-echo [19,81,84,85] in conjunction with cyclic motion-encoding gradients (MEGs). The standard sequences used are GRE-based or EPI-based MRE sequences; at present, 2-D GRE MRE spin-echo EPI MRE methods are used for most clinical applications. MEGs can be applied in the direction of interest and synchronized with the shear wave frequency with a trigger pulse. The shear waves cause cyclic motion of spins that results in phase shifts, which can be measured and depicted on the phase image; this technique is exquisitely sensitive to motion, allowing imaging of displacements in the range of hundreds of nanometers [82]. Alterations can be made in the time offset between the MEGs and the applied waves (phase offset) to allow imaging of the different phases of the wave cycle. Phase images typically are obtained at 4 different time points to capture snapshots of propagation throughout the motion cycle. A typical MRE sequence performed for most hepatic applications can be obtained in 1 minute or less, split into 4 breath holds of approximately 15 seconds, with imaging performed at end-expiration.

ELASTOGRAMS

Postprocessed images from an MRE sequence are presented as a tissue stiffness map, or elastogram, that permits quantitative measure of tissue stiffness in kilopascals. An elastogram often consists of a magnitude image, a phase-contrast image, color and grayscale stiffness maps, a confidence map, and color wave images that can be viewed as a cine (Fig. 5, Table 3). The cine images display the propagation of shear waves and can be used to recognize regions of wave interference. These areas should be avoided when ROIs are drawn on the corresponding grayscale and color stiffness maps [18,20]. ROIs should be placed in the parenchyma, ideally within the right hepatic lobe, with care taken to avoid the edges of the liver and large blood vessels. Data obtained from the left hepatic lobe may be unreliable due to pulsation artifact from adjacent cardiac motion [18]. In cases, however, of excellent propagation of shear waves through the liver, an enlarged left lobe from previous right lobe resection, or anatomic variations in the liver, ROIs may be drawn to include the left lobe to obtain mean liver stiffness. The ROIs should be as large as possible and can be drawn manually or with an automated method where available [86].

APPLICATIONS

With added hardware and postprocessing software, MRE is relatively easy to perform and can be done on any magnet used for routine clinical applications (Box 4). MRE facilitates diagnosis of hepatic fibrosis prior to the development of morphologic changes of cirrhosis and can be used to monitor response to antifibrotic therapy (Fig. 6); unlike serial biopsy, it is noninvasive without risk of significant or life-threatening complications. Compared with ultrasound-based elastography, MRE samples a large fraction of the liver, which is helpful in longitudinal monitoring [81]. Early studies showed that MRE is unaffected by the presence of steatosis and can be performed in both morbidly obese patients and those with ascites [19]. Furthermore, it has been applied successfully to a wide range of

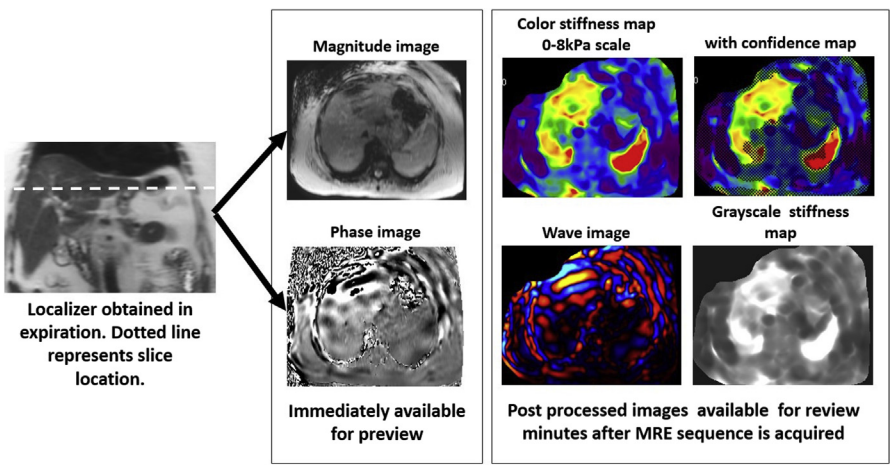

FIG. 5 Illustrative diagram showing a single-slice liver MRE acquisition and postprocessed images.

TABLE 3
Postprocessed Images from Magnetic Resonance Elastography Acquisition

Image Type	Clinical Utility
Magnitude	Provides anatomic information
Phase	Observe pattern of wave propagation through liver
Gray-scale/color maps	Overview of stiffness distribution; measurement of liver stiffness
Color wave images	Observe for areas of wave interference/artifact
Confidence map	Displays crosshatched areas where measurement is less valid

diverse patient populations, including children [87], transplant recipients [88], and patients with unconventional anatomy [19]. Numerous studies have demonstrated that elastography data are reliable across different vendors and magnetic field strengths [89,90]. Data from hepatic MRE also have been shown to be both repeatable and reproducible with excellent interobserver agreement [75,76,91,92] (Box 5).

Potential applications for liver MRE continue to emerge, and, in the future, MRE may be used for differentiation of hepatic masses, distinction of isolated hepatic steatosis from inflammatory steatohepatitis (Fig. 7), and differentiation of inflammation and edema from other pathologic processes. A small study performed at the Mayo Clinic examined 44 hepatic tumors with MRE and found that all malignant masses had a stiffness of at least 5 kPa [93]. MRE is unaffected by the presence of isolated hepatic steatosis but shows increased hepatic stiffness in patients with NASH [94]. In addition, several studies have examined characteristic patterns of increased hepatic stiffness in patients with congestive hepatopathy secondary to heart disease [95] and in patients with primary sclerosing cholangitis [96]. Concomitant measurement of hepatic and splenic stiffness has been performed, with elevated splenic stiffness found to correlate with the presence of portal hypertension and development of esophageal varices [97]. Finally, given its lack of ionizing radiation and safety relative to serial biopsy, MRE probably is the best technique available for serial follow-up of patients with chronic liver disease (Fig. 8).

BOX 4
Current and Future Applications of Magnetic Resonance Elastography

- Diagnosis and staging of hepatic fibrosis
- Longitudinal monitoring of chronic disease
  - Changes in hepatic stiffness over time
  - Response to therapy
- Differentiation of steatosis from steatohepatitis with/without fibrosis
- Characterization of hepatic masses
- Specific patterns/distributions of increased stiffness may indicate etiology
  - For example, peripheral fibrosis in primary sclerosing cholangitis and passive venous congestion
- Simultaneous stiffness measurements in multiple abdominal organs
  - For example, splenic stiffness as a predictor of portal hypertension and development of esophageal varices

ADVANCES IN LIVER MAGNETIC RESONANCE ELASTOGRAPHY

The current clinical standard 2-D-GRE MRE and spin-echo MRE sequences provide liver stiffness measurements based on the assumption that shear waves are propagating in the plane of acquisition (ie, axial) (Box 6). Shear waves travel in different directions, however, and 2-D MRE sequences may overestimate liver stiffness [98]. 3-D MRE can provide better evaluation by enabling motion encoding in all 3 dimensions. Liver stiffness evaluated with 3-D MRE usually is less than that assessed with 2-D technique, because it corrects for obliquity of wave propagation that can lead to overestimation. 3-D MRE is spin-echo based with shorter echo time and, therefore, has better performance in iron deposition [99].

Mechanical properties of tissues are dependent on tissue components and their relative composition. Inflammation and increased venous pressure and increased biliary pressure can affect hepatic stiffness. Multifrequency MRE may be useful in differentiation of various pathologic processes that characterize chronic liver diseases. Multifrequency MRE also improves differentiation of steatohepatitis from simple steatosis. More applications of multifrequency MRE are likely to emerge in the future.

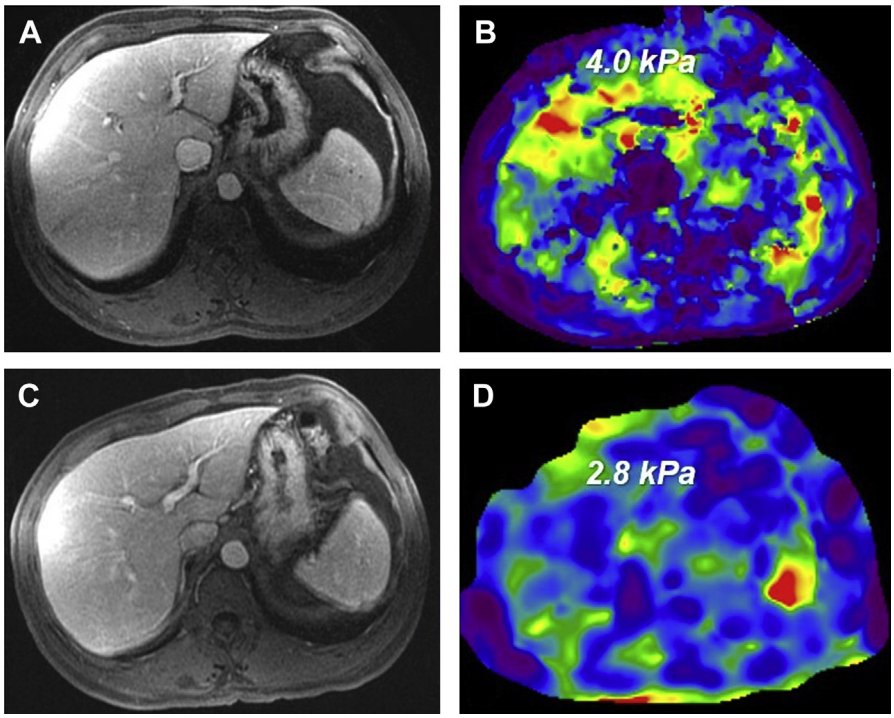

FIG. 6 Liver MRE in the follow-up of chronic liver disease. (**A**) Contrast-enhanced image and (**B**) MRE stiffness map before antiviral therapy showing mean stiffness of 4.0 kPa. Three years after therapy, (**C**) contrast-enhanced image shows no significant change; (**D**) MRE, however, shows improvement in mean stiffness to 2.8 kPa.

BOX 5
Advantages of Magnetic Resonance Elastography

- Can be performed on any clinical scanner with added hardware and postprocessing software
- Noninvasive
- Unaffected by field strength, vendor, and most patient factors (eg, obesity)
- Allows for diagnosis of fibrosis prior to morphologic changes of cirrhosis
- Can be applied to a wide range of patient populations (eg, children, transplant recipients, altered anatomy)
- Well validated, repeatable, and reproducible with excellent interobserver agreement
- Concomitant stiffness measurements of multiple abdominal organs

LIMITATIONS

Standard liver MRE performed with a GRE sequence is susceptible to failure in patients with hepatic iron overload (Box 7) [81]. The reason for failure is due to poor liver signal, which can be improved with a reduced echo time using a spin-echo sequence [100,101]. In cases of severe iron deposition in the liver, however, this method also can fail. Liver stiffness also is affected or modified by the presence of venous congestion, inflammation, biliary obstruction, and diffuse infiltrative diseases other than fibrosis, such as amyloidosis. Clinical features and supportive laboratory data are useful in identifying these possible confounders, and MRE should not be performed for fibrosis evaluation when they coexist or are suspected. MRE also may be suboptimal in patients with inconsistent breath holds [81] and is not yet widely available outside of large academic centers. Free-breathing MRE techniques are being explored and show promise for use in patients who are unable to maintain a breath hold [102].

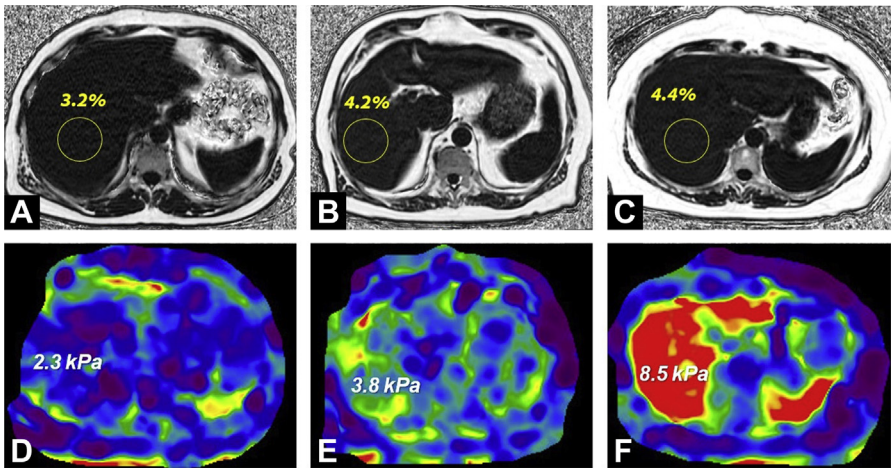

FIG. 7 PDFF maps (*A–C*) and corresponding MRE stiffness maps (*D–E*) in patients with biopsy-proved normal liver parenchyma (first column, *A,D*), NASH (second column, *B, E*), and cirrhosis due to NASH (third column, *C, F*). Note similar PDFF in all 3 subjects but different hepatic stiffness values.

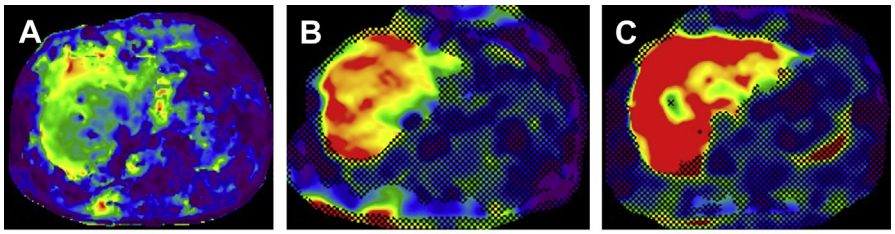

FIG. 8 Liver MRE in the follow-up of chronic liver disease. (**A**) Baseline, (**B**) 2-year, and (**C**) 4-year follow-up MRE stiffness maps obtained in a patient with chronic hepatitis C. Note increase in stiffness of the liver, consistent with progression of disease.

BOX 6
Advances in Magnetic Resonance Elastography

- 3-D MRE
  - Larger volume of liver evaluated (entire liver is possible)
  - Corrects for obliquity of wave propagation and may provide more accurate measurements
- 3-D MRE is spin-echo based with shorter echo time, improving performance in patients with hepatic iron deposition
- Multifrequency MRE
  - Improved differentiation of steatosis from steatohepatitis
  - May allow differentiation of various pathologic processes (eg, inflammation and increased venous or biliary pressure)

BOX 7
Limitations of Magnetic Resonance Elastography

- Standard liver MRE is performed with a GRE sequence
  - Susceptible to failure in patients with hepatic iron overload
- Liver stiffness can be affected by venous congestion, inflammation, and infiltrative diseases, such as amyloidosis
  - Clinical history and laboratory data may be helpful in identifying confounders
- MRE may be suboptimal in patients with inconsistent breath holds
  - Free-breathing techniques are in development and have shown promise

SUMMARY

Over the past decade, CSE-MRI and MRE have emerged as accurate, reproducible, and repeatable means of quantitatively assessing hepatic steatosis and fibrosis. Application of these noninvasive imaging techniques may obviate liver biopsy and its associated complications in some clinical scenarios. As these techniques are refined, they may allow for earlier and even more accurate diagnosis of hepatic pathology, which could facilitate treatment of chronic liver disease and improve long-term patient outcomes.

REFERENCES

[1] Reeder SB, Cruite I, Hamilton G, et al. Quantitative assessment of liver fat with magnetic resonance imaging and spectroscopy. J Magn Reson Imaging 2011;34(4):spcone.

[2] Adams LA, Lymp JF, St Sauver J, et al. The natural history of nonalcoholic fatty liver disease: a population-based cohort study. Gastroenterology 2005;129(1):113–21.

[3] Browning JD, Szczepaniak LS, Dobbins R, et al. Prevalence of hepatic steatosis in an urban population in the United States: impact of ethnicity. Hepatology 2004;40(6):1387–95.

[4] Farrell GC, Larter CZ. Nonalcoholic fatty liver disease: from steatosis to cirrhosis. Hepatology 2006;43(2 Suppl 1):S99–112.

[5] Rinella ME. Nonalcoholic fatty liver disease: a systematic review. JAMA 2015;313(22):2263–73.

[6] Schuppan D, Afdhal NH. Liver cirrhosis. Lancet 2008;371(9615):838–51.

[7] Scaglione S, Kliethermes S, Cao G, et al. The epidemiology of cirrhosis in the United States: a population-based Study. J Clin Gastroenterol 2015;49(8):690–6.

[8] Nusrat S, Khan MS, Fazili J, et al. Cirrhosis and its complications: evidence based treatment. World J Gastroenterol 2014;20(18):5442–60.

[9] Fowell AJ, Iredale JP. Emerging therapies for liver fibrosis. Dig Dis 2006;24(1–2):174–83.

[10] Friedman SL, Bansal MB. Reversal of hepatic fibrosis – fact or fantasy? Hepatology 2006;43(2 Suppl 1):S82–8.

[11] Rockey DC, Caldwell SH, Goodman ZD, et al, American Association for the Study of Liver Diseases. Liver biopsy. Hepatology 2009;49(3):1017–44.

[12] Bravo AA, Sheth SG, Chopra S. Liver biopsy. N Engl J Med 2001;344(7):495–500.

[13] Ratziu V, Charlotte F, Heurtier A, et al. Sampling variability of liver biopsy in nonalcoholic fatty liver disease. Gastroenterology 2005;128(7):1898–906.

[14] Bedossa P, Dargere D, Paradis V. Sampling variability of liver fibrosis in chronic hepatitis C. Hepatology 2003;38(6):1449–57.

[15] Merli M, Galli L, Castagna A, et al. Diagnostic accuracy of APRI, FIB-4 and Forns for the detection of liver cirrhosis in HIV/HCV-coinfected patients. New Microbiol 2016;39(2):110–3.

[16] Kelly ML, Riordan SM, Bopage R, et al. Capacity of noninvasive hepatic fibrosis algorithms to replace transient elastography to exclude cirrhosis in people with hepatitis C virus infection: a multi-centre observational study. PLoS One 2018;13(2):e0192763.

[17] Talwalkar JA, Yin M, Fidler JL, et al. Magnetic resonance imaging of hepatic fibrosis: emerging clinical applications. Hepatology 2008;47(1):332–42.

[18] Venkatesh SK, Ehman RL. Magnetic resonance elastography of liver. Magn Reson Imaging Clin N Am 2014;22(3):433–46.

[19] Venkatesh SK, Yin M, Ehman RL. Magnetic resonance elastography of liver: technique, analysis, and clinical applications. J Magn Reson Imaging 2013;37(3):544–55.

[20] Venkatesh SK, Yin M, Ehman RL. Magnetic resonance elastography of liver: clinical applications. J Comput Assist Tomogr 2013;37(6):887–96.

[21] Reeder SB, Hu HH, Sirlin CB. Proton density fat-fraction: a standardized MR-based biomarker of tissue fat concentration. J Magn Reson Imaging 2012;36(5):1011–4.

[22] Reeder SB, Sirlin CB. Quantification of liver fat with magnetic resonance imaging. Magn Reson Imaging Clin N Am 2010;18(3):337–57, ix.

[23] Puchner SB, Lu MT, Mayrhofer T, et al. High-risk coronary plaque at coronary CT angiography is associated with nonalcoholic fatty liver disease, independent of coronary plaque and stenosis burden: results from the ROMICAT II trial. Radiology 2015;274(3):693–701.

[24] Sung KC, Jeong WS, Wild SH, et al. Combined influence of insulin resistance, overweight/obesity, and fatty liver as risk factors for type 2 diabetes. Diabetes Care 2012;35(4):717–22.

[25] Adams LA, Waters OR, Knuiman MW, et al. NAFLD as a risk factor for the development of diabetes and the metabolic syndrome: an eleven-year follow-up study. Am J Gastroenterol 2009;104(4):861–7.

[26] Lonardo A, Ballestri S, Marchesini G, et al. Nonalcoholic fatty liver disease: a precursor of the metabolic syndrome. Dig Liver Dis 2015;47(3):181–90.

[27] Brunt EM, Janney CG, Di Bisceglie AM, et al. Nonalcoholic steatohepatitis: a proposal for grading and staging the histological lesions. Am J Gastroenterol 1999;94(9):2467–74.

[28] El-Badry AM, Breitenstein S, Jochum W, et al. Assessment of hepatic steatosis by expert pathologists: the end of a gold standard. Ann Surg 2009;250(5):691–7.

[29] Thomsen C, Becker U, Winkler K, et al. Quantification of liver fat using magnetic resonance spectroscopy. Magn Reson Imaging 1994;12(3):487–95.

[30] Longo R, Pollesello P, Ricci C, et al. Proton MR spectroscopy in quantitative in vivo determination of fat

content in human liver steatosis. J Magn Reson Imaging 1995;5(3):281–5.
[31] Longo R, Ricci C, Masutti F, et al. Fatty infiltration of the liver. Quantification by 1H localized magnetic resonance spectroscopy and comparison with computed tomography. Invest Radiol 1993;28(4):297–302.
[32] Szczepaniak LS, Babcock EE, Schick F, et al. Measurement of intracellular triglyceride stores by H spectroscopy: validation in vivo. Am J Physiol 1999;276(5 Pt 1):E977–89.
[33] Yokoo T, Serai SD, Pirasteh A, et al. Linearity, bias, and precision of hepatic proton density fat fraction measurements by using MR imaging: a meta-analysis. Radiology 2018;286(2):486–98.
[34] Dixon WT. Simple proton spectroscopic imaging. Radiology 1984;153(1):189–94.
[35] Borra RJ, Salo S, Dean K, et al. Nonalcoholic fatty liver disease: rapid evaluation of liver fat content with in-phase and out-of-phase MR imaging. Radiology 2009; 250(1):130–6.
[36] Yoshimitsu K, Kuroda Y, Nakamuta M, et al. Noninvasive estimation of hepatic steatosis using plain CT vs. chemical-shift MR imaging: significance for living donors. J Magn Reson Imaging 2008;28(3): 678–84.
[37] O'Regan DP, Callaghan MF, Wylezinska-Arridge M, et al. Liver fat content and T2*: simultaneous measurement by using breath-hold multiecho MR imaging at 3.0 T–feasibility. Radiology 2008;247(2):550–7.
[38] Hussain HK, Chenevert TL, Londy FJ, et al. Hepatic fat fraction: MR imaging for quantitative measurement and display–early experience. Radiology 2005;237(3): 1048–55.
[39] Qayyum A, Goh JS, Kakar S, et al. Accuracy of liver fat quantification at MR imaging: comparison of out-of-phase gradient-echo and fat-saturated fast spin-echo techniques–initial experience. Radiology 2005;237(2): 507–11.
[40] Bydder M, Yokoo T, Hamilton G, et al. Relaxation effects in the quantification of fat using gradient echo imaging. Magn Reson Imaging 2008;26(3):347–59.
[41] Yokoo T, Bydder M, Hamilton G, et al. Nonalcoholic fatty liver disease: diagnostic and fat-grading accuracy of low-flip-angle multiecho gradient-recalled-echo MR imaging at 1.5 T. Radiology 2009;251(1):67–76.
[42] Mitchell DG, Kim I, Chang TS, et al. Fatty liver. Chemical shift phase-difference and suppression magnetic resonance imaging techniques in animals, phantoms, and humans. Invest Radiol 1991;26(12):1041–52.
[43] Fishbein MH, Gardner KG, Potter CJ, et al. Introduction of fast MR imaging in the assessment of hepatic steatosis. Magn Reson Imaging 1997;15(3):287–93.
[44] Reeder SB, McKenzie CA, Pineda AR, et al. Water-fat separation with IDEAL gradient-echo imaging. J Magn Reson Imaging 2007;25(3):644–52.
[45] Kim H, Taksali SE, Dufour S, et al. Comparative MR study of hepatic fat quantification using single-voxel proton spectroscopy, two-point dixon and three-point IDEAL. Magn Reson Med 2008;59(3):521–7.
[46] Liu CY, McKenzie CA, Yu H, et al. Fat quantification with IDEAL gradient echo imaging: correction of bias from T(1) and noise. Magn Reson Med 2007;58(2): 354–64.
[47] Yu H, McKenzie CA, Shimakawa A, et al. Multiecho reconstruction for simultaneous water-fat decomposition and T2* estimation. J Magn Reson Imaging 2007; 26(4):1153–61.
[48] Yu H, Shimakawa A, McKenzie CA, et al. Multiecho water-fat separation and simultaneous R2* estimation with multifrequency fat spectrum modeling. Magn Reson Med 2008;60(5):1122–34.
[49] Reeder SB, Robson PM, Yu H, et al. Quantification of hepatic steatosis with MRI: the effects of accurate fat spectral modeling. J Magn Reson Imaging 2009;29(6): 1332–9.
[50] Kuhn JP, Hernando D, Meffert PJ, et al. Proton-density fat fraction and simultaneous R2* estimation as an MRI tool for assessment of osteoporosis. Eur Radiol 2013; 23(12):3432–9.
[51] Hernando D, Cook RJ, Diamond C, et al. Magnetic susceptibility as a B0 field strength independent MRI biomarker of liver iron overload. Magn Reson Med 2013;70(3):648–56.
[52] Hernando D, Levin YS, Sirlin CB, et al. Quantification of liver iron with MRI: state of the art and remaining challenges. J Magn Reson Imaging 2014;40(5): 1003–21.
[53] Hernando D, Kramer JH, Reeder SB. Multipeak fat-corrected complex R2* relaxometry: theory, optimization, and clinical validation. Magn Reson Med 2013; 70(5):1319–31.
[54] Tang A, Tan J, Sun M, et al. Nonalcoholic fatty liver disease: MR imaging of liver proton density fat fraction to assess hepatic steatosis. Radiology 2013;267(2): 422–31.
[55] Henninger B, Kremser C, Rauch S, et al. Evaluation of liver fat in the presence of iron with MRI using T2* correction: a clinical approach. Eur Radiol 2013;23(6): 1643–9.
[56] Rehm JL, Wolfgram PM, Hernando D, et al. Proton density fat-fraction is an accurate biomarker of hepatic steatosis in adolescent girls and young women. Eur Radiol 2015;25(10):2921–30.
[57] Achmad E, Yokoo T, Hamilton G, et al. Feasibility of and agreement between MR imaging and spectroscopic estimation of hepatic proton density fat fraction in children with known or suspected nonalcoholic fatty liver disease. Abdom Imaging 2015;40(8):3084–90.
[58] Motosugi U, Hernando D, Bannas P, et al. Quantification of liver fat with respiratory-gated quantitative chemical shift encoded MRI. J Magn Reson Imaging 2015;42(5):1241–8.
[59] Hines CD, Frydrychowicz A, Hamilton G, et al. T(1) independent, T(2) (*) corrected chemical shift based

fat-water separation with multi-peak fat spectral modeling is an accurate and precise measure of hepatic steatosis. J Magn Reson Imaging 2011;33(4):873–81.
[60] Bannas P, Kramer H, Hernando D, et al. Quantitative magnetic resonance imaging of hepatic steatosis: validation in ex vivo human livers. Hepatology 2015;62(5):1444–55.
[61] Campo CA, Hernando D, Schubert T, et al. Standardized approach for ROI-based measurements of proton density fat fraction and R2* in the liver. AJR Am J Roentgenol 2017;209(3):592–603.
[62] Szczepaniak LS, Nurenberg P, Leonard D, et al. Magnetic resonance spectroscopy to measure hepatic triglyceride content: prevalence of hepatic steatosis in the general population. Am J Physiol Endocrinol Metab 2005;288(2):E462–8.
[63] Nasr P, Forsgren MF, Ignatova S, et al. Quantification of liver fat content: diagnostic evaluation of proton magnetic resonance spectroscopy compared with histological methods. J Hepatol 2016;64:S493.
[64] Reeder SB. Emerging quantitative magnetic resonance imaging biomarkers of hepatic steatosis. Hepatology 2013;58(6):1877–80.
[65] Hines CD, Yu H, Shimakawa A, et al. T1 independent, T2* corrected MRI with accurate spectral modeling for quantification of fat: validation in a fat-water-SPIO phantom. J Magn Reson Imaging 2009;30(5):1215–22.
[66] Hines CD, Yu H, Shimakawa A, et al. Quantification of hepatic steatosis with 3-T MR imaging: validation in ob/ob mice. Radiology 2010;254(1):119–28.
[67] Meisamy S, Hines CD, Hamilton G, et al. Quantification of hepatic steatosis with T1-independent, T2-corrected MR imaging with spectral modeling of fat: blinded comparison with MR spectroscopy. Radiology 2011;258(3):767–75.
[68] Yokoo T, Shiehmorteza M, Hamilton G, et al. Estimation of hepatic proton-density fat fraction by using MR imaging at 3.0 T. Radiology 2011;258(3):749–59.
[69] Pooler BD, Hernando D, Ruby JA, et al. Validation of a motion-robust 2D sequential technique for quantification of hepatic proton density fat fraction during free breathing. J Magn Reson Imaging 2018;48(6):1578–85.
[70] Motosugi U, Hernando D, Wiens C, et al. High SNR acquisitions improve the repeatability of liver fat quantification using confounder-corrected chemical shift-encoded MR imaging. Magn Reson Med Sci 2017;16(4):332–9.
[71] Angulo P, Kleiner DE, Dam-Larsen S, et al. Liver fibrosis, but no other histologic features, is associated with long-term outcomes of patients with nonalcoholic fatty liver disease. Gastroenterology 2015;149(2):389–97.e10.
[72] Yin M, Talwalkar JA, Glaser KJ, et al. Assessment of hepatic fibrosis with magnetic resonance elastography. Clin Gastroenterol Hepatol 2007;5(10):1207–13.e2.
[73] Ichikawa S, Motosugi U, Ichikawa T, et al. Magnetic resonance elastography for staging liver fibrosis in chronic hepatitis C. Magn Reson Med Sci 2012;11(4):291–7.
[74] Mannelli L, Godfrey E, Graves MJ, et al. Magnetic resonance elastography: feasibility of liver stiffness measurements in healthy volunteers at 3T. Clin Radiol 2012;67(3):258–62.
[75] Lee Y, Lee JM, Lee JE, et al. MR elastography for noninvasive assessment of hepatic fibrosis: reproducibility of the examination and reproducibility and repeatability of the liver stiffness value measurement. J Magn Reson Imaging 2014;39(2):326–31.
[76] Venkatesh SK, Wang G, Teo LL, et al. Magnetic resonance elastography of liver in healthy Asians: normal liver stiffness quantification and reproducibility assessment. J Magn Reson Imaging 2014;39(1):1–8.
[77] Huwart L, Sempoux C, Vicaut E, et al. Magnetic resonance elastography for the noninvasive staging of liver fibrosis. Gastroenterology 2008;135(1):32–40.
[78] Asbach P, Klatt D, Schlosser B, et al. Viscoelasticity-based staging of hepatic fibrosis with multifrequency MR elastography. Radiology 2010;257(1):80–6.
[79] Choi YR, Lee JM, Yoon JH, et al. Comparison of magnetic resonance elastography and gadoxetate disodium-enhanced magnetic resonance imaging for the evaluation of hepatic fibrosis. Invest Radiol 2013;48(8):607–13.
[80] Kim BH, Lee JM, Lee YJ, et al. MR elastography for noninvasive assessment of hepatic fibrosis: experience from a tertiary center in Asia. J Magn Reson Imaging 2011;34(5):1110–6.
[81] Tang A, Cloutier G, Szeverenyi NM, et al. Ultrasound elastography and MR elastography for assessing liver fibrosis: part 1, principles and techniques. AJR Am J Roentgenol 2015;205(1):22–32.
[82] Mariappan YK, Glaser KJ, Ehman RL. Magnetic resonance elastography: a review. Clin Anat 2010;23(5):497–511.
[83] Muthupillai R, Lomas DJ, Rossman PJ, et al. Magnetic resonance elastography by direct visualization of propagating acoustic strain waves. Science 1995;269(5232):1854–7.
[84] Klatt D, Asbach P, Rump J, et al. In vivo determination of hepatic stiffness using steady-state free precession magnetic resonance elastography. Invest Radiol 2006;41(12):841–8.
[85] Asbach P, Klatt D, Hamhaber U, et al. Assessment of liver viscoelasticity using multifrequency MR elastography. Magn Reson Med 2008;60(2):373–9.
[86] Dzyubak B, Venkatesh SK, Manduca A, et al. Automated liver elasticity calculation for MR elastography. J Magn Reson Imaging 2016;43(5):1055–63.
[87] Binkovitz LA, El-Youssef M, Glaser KJ, et al. Pediatric MR elastography of hepatic fibrosis: principles, technique and early clinical experience. Pediatr Radiol 2012;42(4):402–9.
[88] Lee VS, Miller FH, Omary RA, et al. Magnetic resonance elastography and biomarkers to assess fibrosis from

recurrent hepatitis C in liver transplant recipients. Transplantation 2011;92(5):581–6.

[89] Serai SD, Yin M, Wang H, et al. Cross-vendor validation of liver magnetic resonance elastography. Abdom Imaging 2015;40(4):789–94.

[90] Yasar TK, Wagner M, Bane O, et al. Interplatform reproducibility of liver and spleen stiffness measured with MR elastography. J Magn Reson Imaging 2016;43(5):1064–72.

[91] Hines CD, Bley TA, Lindstrom MJ, et al. Repeatability of magnetic resonance elastography for quantification of hepatic stiffness. J Magn Reson Imaging 2010;31(3):725–31.

[92] Wang K, Manning P, Szeverenyi N, et al. Repeatability and reproducibility of 2D and 3D hepatic MR elastography with rigid and flexible drivers at end-expiration and end-inspiration in healthy volunteers. Abdom Radiol (NY) 2017;42(12):2843–54.

[93] Venkatesh SK, Yin M, Glockner JF, et al. MR elastography of liver tumors: preliminary results. AJR Am J Roentgenol 2008;190(6):1534–40.

[94] Chen J, Talwalkar JA, Yin M, et al. Early detection of nonalcoholic steatohepatitis in patients with nonalcoholic fatty liver disease by using MR elastography. Radiology 2011;259(3):749–56.

[95] Serai SD, Wallihan DB, Venkatesh SK, et al. Magnetic resonance elastography of the liver in patients status-post fontan procedure: feasibility and preliminary results. Congenit Heart Dis 2014;9(1):7–14.

[96] Eaton JE, Dzyubak B, Venkatesh SK, et al. Performance of magnetic resonance elastography in primary sclerosing cholangitis. J Gastroenterol Hepatol 2016;31(6):1184–90.

[97] Talwalkar JA, Yin M, Venkatesh S, et al. Feasibility of in vivo MR elastographic splenic stiffness measurements in the assessment of portal hypertension. AJR Am J Roentgenol 2009;193(1):122–7.

[98] Hoodeshenas S, Yin M, Venkatesh SK. Magnetic resonance elastography of liver: current update. Top Magn Reson Imaging 2018;27(5):319–33.

[99] Morisaka H, Motosugi U, Glaser KJ, et al. Comparison of diagnostic accuracies of two- and three-dimensional MR elastography of the liver. J Magn Reson Imaging 2017;45(4):1163–70.

[100] Wang J, Glaser KJ, Zhang T, et al. Assessment of advanced hepatic MR elastography methods for susceptibility artifact suppression in clinical patients. J Magn Reson Imaging 2018;47(4):976–87.

[101] Serai SD, Trout AT. Can MR elastography be used to measure liver stiffness in patients with iron overload? Abdom Radiol (NY) 2018;44(1):104–9.

[102] Morin CE, Dillman JR, Serai SD, et al. Comparison of standard breath-held, free-breathing, and compressed sensing 2D gradient-recalled echo MR elastography techniques for evaluating liver stiffness. AJR Am J Roentgenol 2018;211(6):W279–87.